Supplement of

Annual high-resolution grazing intensity maps on the Qinghai-Tibet Plateau from 1990 to 2020

Jia zhou, Jin Niu, Ning Wu, Tao Lu

Correspondence to: Tao Lu (lutao@cib.ac.cn)

Supplementary Methods

There is a conspicuous absence of a systematic database with superior spatio-temporal resolution, including population density, temperature, precipitation, and Human-activity-induced Net Primary Productivity (HNPP). The lack of such a comprehensive dataset significantly compromises the empirical robustness of research endeavors in the domain of livestock distribution mapping. Consequently, this study is committed to providing precise and detailed mappings that integrate the aforementioned elements. The subsequent section demonstrated the methodologies employed to generate these comprehensive maps.

Population density database

Data source. The gridded annual population data with a resolution of 100 m spanning from 2000 to 2020 (referred to as Pop I) for this study were acquired from the WorldPop dataset (https://hub.worldpop.org, accessed on 5 January 2023). Concurrently, the gridded population data at 1 km resolution with five-year intervals for the period of 1990-2015 (referred to as Pop II) were obtained from the Resource and Environment Science and Data center of the Chinese Academy of Sciences (https://www.resdc.cn, accessed on 9 January 2023). Moreover, the demographic data spanning the years 1990-2000 were extracted from the statistical yearbooks of the respective provinces.

Data processing. All collected gridded population data were meticulously geo-referenced to the WGS_1984_Albers Equal-Area Conic coordinate system, and were subsequently clipped by the comprehensive boundary of the entire Qinghai-Tibetan Plateau (QTP). Furthermore, the PopII dataset was aggregated to a 100 m resolution to maintain consistency. Given the inherent disparities between the Pop I and Pop II datasets—originating from distinct demographic data and divergent methodologies—an integration process was required to prevent data breakage and ensure continuity across datasets. In this study, for the overlapping year of 2000-2015, both Pop I and Pop II data were harmoniously amalgamated to construct a linear regression model, according to the formula 1~3. Subsequently, consistent gridded population data with a spatial resolution of 100 m × 100 m, were generated for the years 1990 to 1999, undergoing stringent quality control procedures utilizing the acquired demographic data.

$$y = ax + b \tag{1}$$

$$a = \frac{\sum_{i=1}^{n}(x_i - \bar{x})(y_i - \bar{y})}{\sum_{i=1}^{n}(x_i - \bar{x})} \tag{2}$$

$$b = \bar{y} - a\bar{x} \tag{3}$$

where y is Pop I, X is Pop II, and n is the number of samples.

Climate database

Data source. In the present study, the mean daily temperature and precipitation data of 228 meteorological stations in the QTP and its surrounding areas during 1990-2020 were obtained from China Meteorological Data Service Center (http://data.cma.cn, accessed on 4 January 2023). The quality and uniformity of the acquired data were assessed and validated by the National Meteorological Information Center, ensuring the reliability and consistency of the datasets in use.

Data processing. To avoid the influence of anomalous values, average values were selected for interpolation of air temperature, while interpolation of precipitation incorporated total values (Bryan and Adams, 2002). Subsequent to the exclusion of abnormal data, the annual average temperature and the annual cumulative precipitation for each station were ascertained. Previous studies reveals that both the ANUSPLIN and Co-Kriging methodologies are typically conducive to generating robust and reliable estimations for climatic data (Parra and Monahan 2008, Cho et al. 2020, Tan et al. 2021). Consequently, after comparing the results from all possible parameter combinations, eight models were constructed with three independent variables, including altitude, slope, and aspect, as detailed in Table S1.

The ANUSPLIN model serves as an advanced interpolation technique, proficient in generating geographically cohesive climate surfaces, utilizing both weather station data and topographical variables. This model is constructed employing thin-plate smoothing splines, demonstrating a notable suitability for interpolating climate data characterized by substantial noise, whilst maintaining a propensity to yield a mean error that is lower compared to alternate interpolation models (Price et al., 2000; Hutchinson, 2005). The theoretical framework underpinning this model is articulated through Formula (4), serving as a testament to its mathematical robustness and empirical reliability in addressing the complexities inherent to climatic data.

$$Z_i = f(x_i) + b^T y_i + e_i \qquad (i=1,\ldots,n) \tag{4}$$

where Z_i represents the predicted value at location i; x_i is the spline independent variable as a multidimensional vector, and f represents a smoothing function of x_i which needs to be estimated; y_i is the independent covariable as a multidimensional vector, and b is the unknown coefficients for the y_i; n is the number of observational data. Each e_i is an independent, zero mean error term with variance $w_i\sigma^2$, where w_i is the known relative error variance and σ^2 is the error variance which is constant across all data points.

Co-Kriging represents a sophisticated multivariate geostatistical technique, functioning as an advanced extension of the Ordinary Kriging method, and is adept at transitioning from a singular spatial random variable to encompassing multiple spatially correlated random variables. This technique incorporates multiple correlated datasets into the estimation process, typically resulting in predictions characterized by enhanced accuracy (Tajgardan et al., 2010). The mathematical theory underpinning Co-Kriging is delineated in Formula (5).

$$Z^*(x_0) = \sum_{i=1}^{n_1} \beta_{1i} Z_1(x_{1i}) + \sum_{j=1}^{n_2} \beta_{2j} Z_2(x_{2j}) + \sum_{p=1}^{n_3} \beta_{3p} Z_3(x_{3p}) + \sum_{q=1}^{n_4} \beta_{4q} Z_4(x_{4q}) \tag{5}$$

where $Z^*(X_0)$ is the simulated value of the point X_0 to be evaluated, the measured climate value of Z_1 (x_{1i}) is taken as the main variable, and Z_2 (x_{2j}), Z_3 (3_i) and Z_4 (x_{4i}) are taken as the covariates; β represents the weight; n represents the number of data; X_i, X_J, X_P and Xq represent the location, and $I = 1, 2, 3.. n1$, $j=1,2,3\cdots\cdots n2$, $p=1,2,3\cdots\cdots n3$, $q=1,2,3\cdots\cdots n4$.

Table S1. Interpolation models using different combinations of covariates for prediction of air temperature and precipitation

Climate	ANUSPLIN		Co-Kriging	
Temperature	A-T-I	CV：Altitude	K-T-I	CV：Altitude
	A-T-II	CV：Altitude; slope; aspect	K-T-II	CV：Altitude; slope; aspect
Precipitation	A-P-I	CV：Altitude	K-P-I	CV：Altitude
	A-P-II	CV：Altitude; slope; aspect	K-P-II	CV：Altitude; slope; aspect

Note: CV is an abbreviation for concomitant variable

Model assessment. To rigorously evaluate the efficacy of the eight models, we engaged in the construction and assessment of all predictive models utilizing repeated 10-fold cross-validation (Yoo et al., 2018). This method systematically divided the original observation data from the 228 meteorological stations into ten equitably sized subsamples. Nine of these subsamples were deployed in the training process, subsequently generating predictions on the remaining subsample. This cross-validation process was hen repeated a further nine times, ensuring each observation was exclusively used once as validation data. Hence, ten distinctive combinations of training and test sets were established, with each pair undergoing comprehensive application and evaluation. The conclusive assessment of the 10-fold cross-validation was derived from the average error across the ten test sets, culminating in a singular, consolidated estimate.

The mean absolute error (MAE) and the root mean square error (RMSE) were employed as evaluation metrics to quantify the discrepancies between the forecasted data and the actual observed data, serving as indicators of model performance. The MAE and RMSE were computed for 56,544 (228×31×8) samples, as detailed in Table S2, to systematically assess the accuracy of the models. The optimal model was adjudged based on the relative minimization of both MAE and RMSE during the modeling and forecasting stages. The results indicated that the A-T-II model exhibited superior performance in predicting temperature, whereas the K-P-I model demonstrated paramount accuracy in forecasting precipitation. Consequently, the A-T-II and K-P-I models were deployed to construct the annual temperature and precipitation maps of the QTP spanning the period from 1990 to 2020, as illustrated in Figure S1.

Table S2. Model performance for the response prediction models

Climate	Temperature				Precipitation			
Models	A-T-I	A-T-II	K-T-I	K-T-II	A-P-I	A-P-II	K-P-I	K-P-II
Test samples	7068	7068	7068	7068	7068	7068	7068	7068
MAE	1.506	0.998	1.89	1.91	109.509	110.614	99.05	99.47
RMSE	2.75	1.551	2.54	2.55	172.770	175.483	147.28	147.68

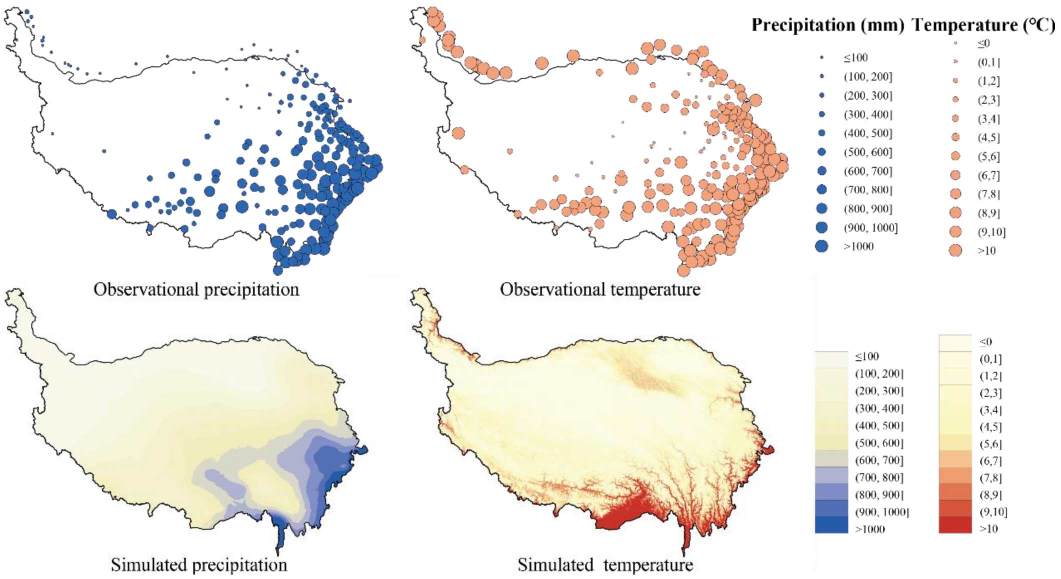

Figure S1. Distribution of mean cumulative precipitation and mean temperature in the QTP as predicted by K-P-I and A-T-II model, respectively

Human-activity-induced Net Primary Productivity (HNPP) database

Data source. The MOD17A3HGF Version 006 NPP product (referred to as NPP-I) with 500 m resolution covering 2000 to 2020 were obtained from the Land Processes Distributed Active Archive Center (https://lpdaac.usgs.gov, accessed on 18 January 2023). Additionally, the actual NPP dataset during 1990-2015 at 1 km resolution (referred to as NPP-II) was derived from the MOD17A3 NPP product (http://www.ntsg.umt.edu, accessed on 22 January 2023).

Data processing. To reconcile the discrepancies inherent between NPP-I and NPP-II datasets, an initial re-projection to the WGS_1984_Albers Equal-Area Conic coordinate system was undertaken. Subsequently, the resolution of NPP-II was resampled to 500-m through the employment of the nearest neighbor resampling algorithm. Based on the NPP-I and NPP-II data for the overlapping year of 2000-2015, a linear regression correction equation was established in accordance with formula 1~3. Consequently, the consistent gridded NPP data (referred to as NPP-III) at 500 m×500 m spatial resolution from 1990 to 2000 was generated.

Human-induced NPP (HNPP) is delineated by the discrepancy between the climate-driven potential NPP (PNPP) and the actual NPP (ANPP). In this study, the NPP-III data epitomize the ANPP, elucidating the extant conditions of vegetative growth. To estimate the PNPP, the Thornthwaite Memorial model was utilized, incorporating temperature and precipitation as determining variables (Naeem et al. 2020; Yin et al. 2020; Qin et al. 2021). Subsequently, the differentiation between PNPP and ANPP was performed to manifest the influence of human activities on NPP. HNPP values in the negative spectrum indicate gains in NPP attributable to anthropogenic activities, while positive values represent losses in NPP due to human interventions. The computations for PNPP and HNPP were conducted as outlined below:

$$\mathrm{PNPP} = 3000\left[1 - \mathrm{e}^{-0.0009695(\mathrm{v}-20)}\right] \quad (6)$$

$$\mathrm{v} = \frac{1.05\mathrm{r}}{\sqrt{1+(1+\frac{1.05\mathrm{r}}{\mathrm{L}})^2}} \quad (7)$$

$$\mathrm{L} = 3000 + 25\mathrm{t} + 0.05\mathrm{t}^3 \quad (8)$$

$$HNPP = PNPP - ANPP \quad (9)$$

where PNPP represents the total annual potential NPP (gC m^{-2}), v represents the annual mean actual evapotranspiration (mm), L represents the annual mean potential evapotranspiration (mm), r represents the annual precipitation (mm) and t represents the average annual temperature (° C).

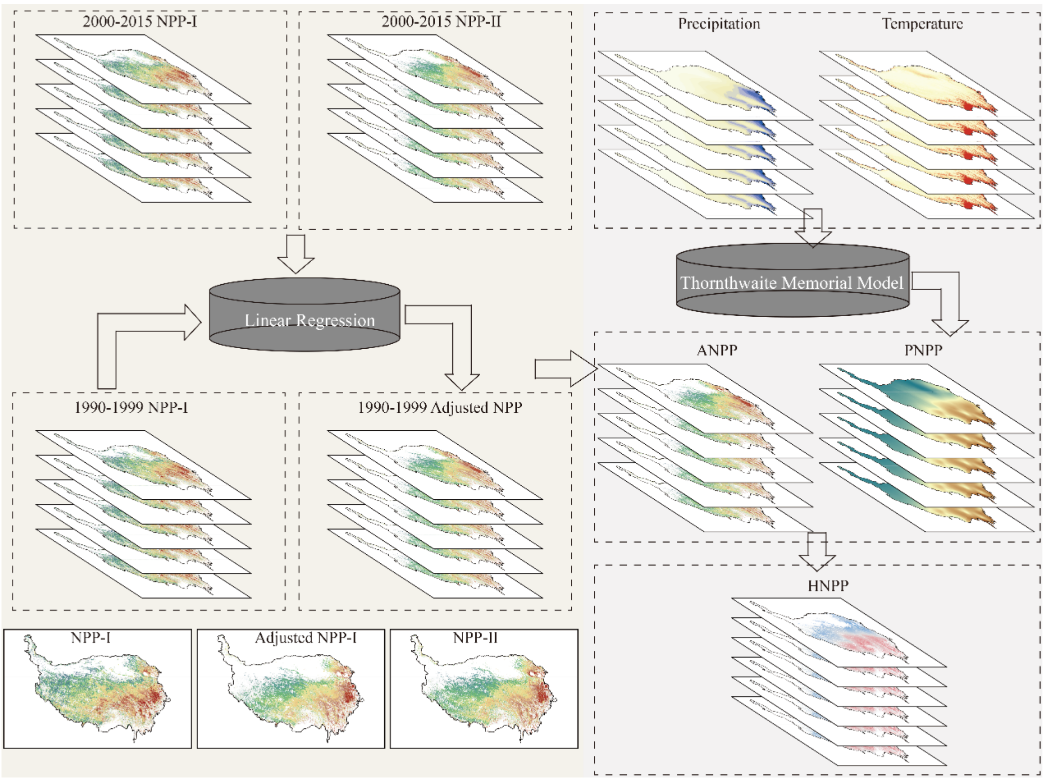

Figure S2. Technical flowchart for mapping the HNPP on the QTP

References

Bryan, B.A. and J.M. Adams. 2002. Three-Dimensional Neurointerpolation of Annual Mean Precipitation and Temperature Surfaces for China. Geographical Analysis 34(2): 93-111.

Cho, D., C.Yoo, J. Im, Y. Lee, and J. Lee. 2020. Improvement of spatial interpolation accuracy of daily maximum air temperature in urban areas using a stacking ensemble technique. GIScience & Remote Sensing **57**:633-649.

Hutchinson, M.F., S. McIntyre, R.J. Hobbs, J.L. Stein, S. Garnett, and J. Kinloch. 2005. Integrating a global agro-climatic classification with bioregional boundaries in Australia. Global Ecology and Biogeography 14: 197-211.

Naeem, S., Y. Zhang, J. Tian, F. M. Qamer, A. Latif, and P. K. Paul. 2020. Quantifying the Impacts of Anthropogenic Activities and Climate Variations on Vegetation Productivity Changes in China from 1985 to 2015. Remote Sensing **12(7)**: 1113.

Parra, J. L., and W. B. Monahan. 2008. Variability in 20th century climate change reconstructions and its consequences for predicting geographic responses of California mammals. Global Change Biology **14**:2215-2231.

Price, D.T., D.W. McKenney, I.A. Nalder, M.F. Hutchinson and J.L. Kesteven. 2000. A comparison of two statistical methods for spatial interpolation of Canadian monthly mean climate date. Agricultural and Forest Meteorology **101**: 81-94.

Qin, X., W. Liu, R. Mao, J. Song, Y. Chen, C. Ma, and M. Li. 2021. Quantitative assessment of driving factors affecting human appropriation of net primary production (HANPP) in the Qilian Mountains, China. Ecological Indicators **121**: 106997.

Tajgardan, T., S. Ayoubi, S. Shataee, K.L. Sahrawat. 2010. Soil Surface Salinity Prediction Using ASTER Data: Comparing Statistical and Geostatistical Models. Australian Journal of Basic and Applied Sciences, **4 (3):** 457-467.

Tan, J., X. Xie, J. Zuo, X. Xing, B. Liu, Q. Xia, and Y. Zhang. 2021. Coupling random forest and inverse distance weighting to generate climate surfaces of precipitation and temperature with Multiple-Covariates. Journal of Hydrology **598**: 126270.

Yoo, C., J. Im, S. Park, L.J. Quackenbush. 2018. Estimation of daily maximum and minimum air temperatures in urban landscapes using MODIS time series satellite data. ISPRS Journal of Photogrammetry and Remote Sensing **137:** 149-162.

Yin, L., E. F. Dai, D. Zheng, Y. H. Wang, L. Ma, and M. Tong. 2020. What Drives the Vegetation Dynamics in the Hengduan Mountain Region, Southwest China: Climate Change or Human Activity? Ecological Indicators **112**:106013.